Journal of Quantitative Spectroscopy & Radiative Transfer 305 (2023) 108626

Contents lists available at ScienceDirect

Journal of Quantitative Spectroscopy & Radiative Transfer

journal homepage: www.elsevier.com/locate/jqsrt

Vacuum UV photoabsorption spectroscopic and photoionization mass spectrometric study of geminal dibromoethylene (1,1-$Br_2C_2H_2$) in the 5–15eV range. Experiment and theory

R. Locht[a,*], D. Dehareng[b]

[a] MolSys Research Unit, Laboratory for Molecular Dynamics, Department of Chemistry, Institute of Chemistry, Blg.B6c, University of Liège, Sart-Tilman B-4000 Liège 1, Belgium

[b] Centre d'Ingéniérie des Protéines, Institute of Chemistry, Bât.B6a, University of Liège, Sart-Tilman B-4000 Liège 1, Belgium

ARTICLE INFO

Article history:
Received 12 January 2023
Revised 19 April 2023
Accepted 21 April 2023
Available online 23 April 2023

ABSTRACT

The vacuum UV photoabsorption spectrum (PAS) of 1,1-$C_2H_2Br_2$ has been examined between 5 eV and 15 eV using the vacuum UV light of synchrotron radiation. For the first time the photoionization mass spectroscopy and efficiency of 1,1-$C_2H_2Br_2^+$ has been measured in the same energy range. A quantum chemical calculation is proposed for the investigation of the neutral and ionized states. The photoionization efficiency curve (PIEC) of 1,1-$C_2H_2Br_2^+$ provided the $IE_{ad}(\tilde{X}^2B_1)$= 9.617±0.005 eV. A vibrational structure gave ω_3^+=1336 cm^{-1} and most likely ω_4^+=483 cm^{-1}. The PIEC of $C_2H_2Br^+$ shows the lowest appearance energy to be at 11.14±0.02 eV. The onset at 11.56±0.01 eV likely corresponds to the excitation of Br in the $^2P_{1/2}$ spin-orbit state. In the vacuum UV-PAS the broad band observed at 6.231 eV includes $n_\sigma \rightarrow Rs$, $2b_1(\pi) \rightarrow \pi^*$ valence transitions and the $2b_1 \rightarrow 3$ s Rydberg transition in agreement with the present calculations. An isolated weak continuum at 7.15 eV is assigned to the $n_\pi \rightarrow \pi^*$ transition. The $2b_1 \rightarrow 3$ s Rydberg transition is characterized by a short progression starting at 6.583 eV. A series of long progressions observed between 7.364 eV and 9.666 eV has been analyzed in terms of vibrational transitions to np- (δ= 0.544) and nd-type (δ= -0.04) Rydberg states all converging to the $\tilde{X}^2B_1$ ionic ground state. An analysis has been attempted providing average values of the vibrational wavenumbers $\omega_3 \approx 1300$ cm^{-1} (or 162 meV), $\omega_4 \approx 480$ cm^{-1} (or 60 meV) and $\omega_5 \approx 145$ cm^{-1} (or 18 meV). By the same way several other Rydberg states were analyzed. For the first time the vacuum UV spectrum of 1,1-$C_2H_2Br_2$ has been recorded above 10 eV and up to 15 eV. Several broad bands are tentatively assigned to transitions to Rydberg states converging to excited ionic states of 1,1-$C_2H_2Br_2^+$. For one of these a vibrational structure is observed and a tentative assignment is proposed.

1. Introduction

The most straightforward reason for the interest in molecular excited states investigation is the occurrence of many chemical reactions through these states. Owing to their importance in many fields of both pure and applied chemistry numerous studies on the spectral properties of the mono-halo-ethylenes have been initiated. During the last three decades this interest was considerably increased by the environmental concern generated by the ozone-depleting effect assigned to the presence of the halogens in the troposphere and stratosphere [1]. For a few of these compounds these investigations were extended to F and/or Cl poly-substituted derivatives of ethylene. The corresponding bromo– and iodo-compounds were seldom considered. In spite of their lower abundance, it has been recognized that bromine and iodine have ozone depleting rates of about 60 and 150–300 times larger than chlorine respectively [1].

The spectroscopic investigations of the 1,1-$C_2H_2Br_2$ are very few. To the best of our knowledge, the only vacuum UV photoabsorption spectrum (PAS) in the region 45,000–90,000 cm^{-1} (220–110 nm or 5.63–11.26 eV) of 1,1-$C_2H_2Br_2$ has been reported by Schander and Russell [2] together with its cis-1,2- and trans-1,2-isomers. Rydberg series analysis and assignments were proposed.

Even scarce is the investigation of the ionization of 1,1-$C_2H_2Br_2$. Wittel and Bock [3] measured the HeI-photoelectron spectrum (PES) of the three $C_2H_2Br_2$ isomers. Von Niessen et al. [4] examined the HeII-PES of the 1,1-$C_2H_2Br_2$ species only. Neither dissociative photoionization nor electroionization work on the 1,1-$C_2H_2Br_2$ has been reported.

* Corresponding author.
E-mail address: robert.locht@uliege.be (R. Locht).

https://doi.org/10.1016/j.jqsrt.2023.108626
0022-4073/

Continuing our work on the halo-ethylenes, the aim of this paper is to report on (i) the photoionization and dissociative ionization of 1,1-$C_2H_2Br_2$ in the 5–15 eV photon energy range and (ii) the vacuum UV photoabsorption spectrum of 1,1-$C_2H_2Br_2$ in the same energy range.

2. Experimental

The experimental setup used in this work has already been described in detail elsewhere [5,6]. Briefly, on the 3m-NIM-2 beamline at the BESSY II facility (Berlin, Germany), a 3m-NIM monochromator equipped with an Al/MgF_2 spherical grating of 600 lines/mm has been used. The entrance and exit slits were adjusted at 40 µm and 10 μm respectively. The vapor pressure in the 30 cm long stainless steel windowless absorption cell is measured by a Balzers capacitor manometer. A sodium salicylate sensitized photomultiplier is used for light detection. The recording of an absorption spectrum requires one scan with gas in the absorption cell and one with the evacuated cell.

The same monochromator has been used for the photoionization mass spectrometry experiments but entrance and exit slits are opened at 200 µm. The light beam focused on the center of an ion chamber is detected by a sodium salicylate sensitized photomultiplier positioned in front of the monochromator exit slit. The ions produced in the ion chamber are mass analyzed by a quadrupole mass spectrometer, detected by a channeltron multiplier and recorded by a 100 MHz counter. The ion signal is automatically normalized to the photon flux at all wavelengths.

Photoabsorption and photoionization efficiency curves often show very weak sharp peaks and diffuse structures superimposed on a strong continuum. To facilitate the characterization of these features a continuum subtraction procedure is applied [7,8]. The underlying continuum is simulated by severely smoothing the experimental curve using the filtering by fast Fourier transform (FFT). This continuum is then subtracted from the original spectrum. The resulting diagram will be called Δ-plot in the forthcoming sections. This data handling has been thoroughly investigated and validated by Marmet and Carbonneau [9].

The monochromator has been calibrated by using the multiple lines PAS of N_2 between 12 eV and 15 eV [10]. The accuracy of this calibration is better than 2 meV. In the measurements between 5 eV and 11 eV, the PAS has been recorded with an energy increment of 0.5 meV. The accuracy on the energy position of a feature is estimated to be 2 meV including the calibration error. Above 11 eV and up to 15 eV an energy increment of 10 meV has been used and a total uncertainty of the order of 5 meV will be adopted.

The commercially available 1,1-$C_2H_2Br_2$ of 98% purity, purchased from ABCR, was used without further purification.

3. Experimental results

3.1. The photoabsorption spectrum of 1,1-$C_2H_2Br_2$

The vacuum UV-PAS of 1,1-$C_2H_2Br_2$ as measured between 5 eV and 11 eV photon energy is represented in Fig. 1 by the extinction coefficient ε ($mol^{-1}.dm^3.cm^{-1}$) as a function of the photon energy (eV). The upper panel of Fig. 2 shows the vacuum UV-PAS as observed between 8 eV and 15 eV. The successive adiabatic or vertical ionization energies measured by HeI-PES [3] are included.

The PAS may be divided in three very different regions: (i) the 5.0–7.3 eV region consisting of a number of very weak broad bands superimposed on a weak continuum, (ii) the 7.3–11 eV region containing a large number of weak to very strong sharp structures and bands superimposed on a continuum with increasing intensity up from 8 eV to about 10 eV and (iii) the region above 11 eV and up to 15 eV consisting of at least four weak broad, likely partly structured, bands superimposed on a strong continuum. Therefore, the latter region is illustrated by a Δ-plot in the lower panel of Fig. 2.

In both figures, vertical bars locate most of the structures and Rydberg series which will be considered in the following discussion. Shaded areas indicate the successive convergence limits. The

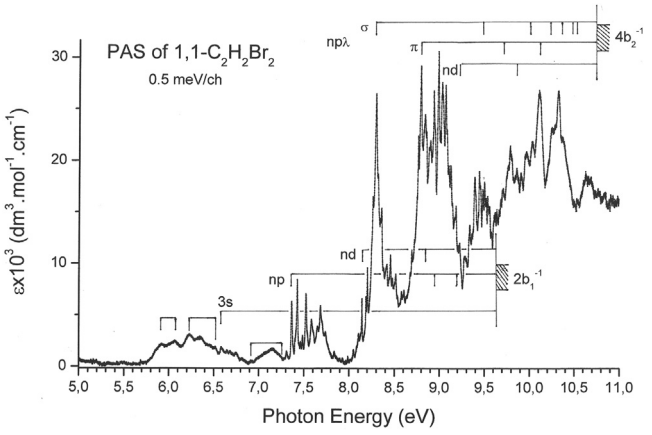

Fig. 1. VUV photoabsorption spectrum of 1,1-$C_2H_2Br_2$ between 5 eV and 11 eV measured with 0.5 meV energy increments. Vertical bars and shaded areas locate only those Rydberg states converging to the first two ionization limits.

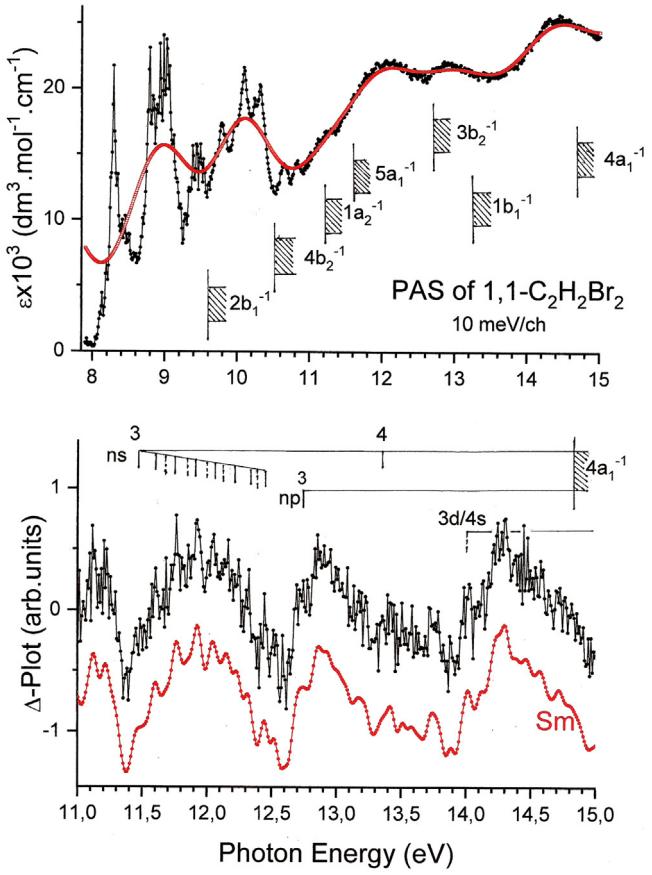

Fig. 2. VUV photoabsorption spectrum of 1,1-$C_2H_2Br_2$ between 8 eV and 15 eV photon energy. The upper panel displays the spectrum as measured with 10 meV energy increments. The shaded areas correspond to the ionization energy values of 1,1-$C_2H_2Br_2$ below 15 eV [3]. The lower panel shows the Δ-plot as a function of the photon energy between 11 and 15 eV (black curve) and slightly smoothed by FFT (red curve Sm). Vertical bars indicate the band maxima and shaded areas correspond to the successive ionization energy values of 1,1-$C_2H_2Br_2$.

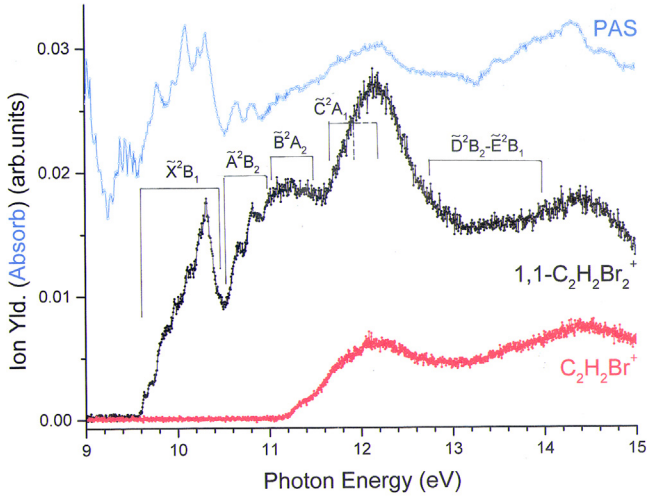

Fig. 3. Photoionization efficiency curves of the 1,1-$C_2H_2Br_2^+$ molecular ion (black curve) and the $C_2H_2Br^+$ fragment ion (red curve) between 9 eV and 15 eV. The photoabsorption spectrum (PAS) measured in the 9–15 eV photon energy range is inserted (blue curve). Vertical bars define the Franck-Condon region of the successive ionic states as observed in the HeI-PES [3].

position in energy of the vibrationless Rydberg transitions converging to the ionic ground state and the successive ionic excited states are listed in Table 1 together with data previously reported by Schander and Russell [2].

3.2. The photoionization of 1,1-$C_2H_2Br_2$

The photoionization efficiency curves (PIEC) of the two most abundant ions in the mass spectrum of 1,1-$C_2H_2Br_2$, i.e. the $C_2H_2Br_2^+$ molecular ion and the $C_2H_2Br^+$ fragment ion, are reproduced in Fig. 3. For helping the forthcoming discussion, the PAS of 1,1-$C_2H_2Br_2$ observed in the 9–15 eV region in the present work is reproduced in the same figure. The Franck-Condon regions covered by the successive ionic states as observed in the HeI-PES [3] are also inserted.

4. Ab initio calculations: methods and results

The molecular orbital configuration of 1,1-$C_2H_2Br_2$ in the C_{2v} symmetry point group is described by

$1s^2(Br1)\ 1s^2(Br2)\ 2s^2(Br1)\ 2s^2(Br2)\ 2p_{x,y,z}{}^6(Br1)\ 2p_{x,y,z}{}^6(Br2)\ 1s^2(C1)\ 1s^2(C2)\ 3s^2(Br1)\ 3s^2(Br2)\ 3p_{x,y,z}{}^6(Br1)\ 3p_{x,y,z}{}^6(Br2)\ 3d^{10}(Br1)\ 3d^{10}(Br2)$

$$1a_1^2 1b_2^2 2a_1^2 3a_1^2 2b_2^2 4a_1^2 1b_1^2 3b_2^2 5a_1^2 1a_2^2 4b_2^2 2b_1^2 : \tilde{X}^1A_1$$

where $1a_1$ is the first outer-valence shell orbital.

4.1. Computational tools

The calculations presented in this work were performed with the Gaussian 09 program [12]. The basis set used for all the calculations is aug-cc-pVDZ [13], containing polarization and diffuse functions.

The geometry optimization was performed at two calculation levels, i.e. the M06–2X(DFT) [14] and TDDFT/M06–2X [15] levels. The vibrational wavenumbers associated with the twelve vibrational normal modes of 1,1-$C_2H_2Br_2$ in the C_{2v} symmetry point group were calculated at DFT/M06–2X and TDDFT/M06–2X levels and are schematically represented in Fig. S1 (see Supplementary material). The shape of virtual and ionized MO's calculated

Table 1
Rydberg series observed in the vacuum UV photoabsorption spectrum of 1,1-$C_2H_2Br_2$ converging to the successive ionized states. Excitation energy (adiabatic or vertical) (eV), wavenumber (cm^{-1}), effective quantum numbers (n^*), average quantum defects ($\bar{\delta}$) and assignments proposed in this work. Comparison is made with available literature data of [2]. Conversion factor: 1 eV= 8 065.545 eV [11].

This work			[2]
eV	cm^{-1}	n^*	(cm^{-1})
Rydb.Ser. convg. to IE_{ad}=9.617 eV[a]			
$2b_1 \rightarrow ns$ ($\bar{\delta}$=0.882)			
6.585	53,112	2.118	53,129
$2b_1 \rightarrow np$ ($\bar{\delta}$=0.545±0.023)			
7.364	59,395	2.457	59,411
8.479	68,388	3.458	69,190
8.939	72,098	4.480	73,137
9.185	74,082	5.612	75,180
$2b_1 \rightarrow nd$ ($\bar{\delta}$= −0.04±0.01)			
8.142	65,670	3.037	*65,673*[c]
8.786	70,848	4.041	*(70,927)*[c]
Rydb.Ser. convg. to IE_{vert}=10.73 eV [3]			
$4b_2 \rightarrow np\sigma$ ($\bar{\delta}$=0.636±0.045)			
8.300	66,944	2.366	66,948
–	–	–	76,589
10.033	80,922	4.418	80,749
10.249	82,664	5.318	82,699
10.396	83,849	6.382	83,808
10.470	84,446	7.233	–
10.531	84,938	8.368	–
$4b_2 \rightarrow np\pi$ ($\bar{\delta}$=0.330±0.026)			
8.798	70,961	2.654	*(70,927)*[c]
9.711	78,325	3.654	*(78,989)*[c]
10.114	81,975	4.700	–
$4b_2 \rightarrow nd$ ($\bar{\delta}$= −0.008±0.002)			
9.224	74,397	3.006	*74,360*[c]
9.884	79,720	4.010	*79,669*[c]
Rydb.Ser. convg. to IE_{ad}=11.23 eV [3]			
$1a_2 \rightarrow ns$ ($\bar{\delta}$=0.997)			
7.839	63,226	2.003	–
9.720	78,397	3.003	*(78,989)*[c]
$1a_2 \rightarrow np$ ($\bar{\delta}$=0.544±0.024)			
8.993	72,533	2.466	–
10.095	81,426	3.465	*(81,018)*[c]
10.550	84,987	4.431	*(84,930)*[c]
10.767	86,842	5.421	*(86,861)*[c]
10.907	87,971	6.490	–
Rydb.Ser.convg.to IE_{ad}=11.60 eV [3]			
$5a_1 \rightarrow ns$ ($\bar{\delta}$=0.998±0.016)			
[8.202][d]	66,154	2.001	–
[10.089][d]	81,373	3.001	*(81,018)*[c]
[10.743][d]	86,648	3.984	*(86,410)*[c]
–	–	–	–
[11.215][d]	90,455	5.945	–
$5a_1 \rightarrow np$ ($\bar{\delta}$=0.487±0.018)			
[9.413][d]	75,921	2.494	*(75,930)*[c]
[10.509][d]	84,761	3.531	*(84,930)*[c]
[10.932][d]	88,172	4.513	–
Rydb.Ser.convg.to IE_{ad}=12.77 eV[b]			
$3b_2 \rightarrow$ 3 s (δ=0.993)			
9.393	75,760	2.007	*(75,930)*[c]
$3b_2 \rightarrow 3p(\sigma)$ (δ=0.640)			
10.327	83,301	2.36	*(83,500)*[c]
Rydb.Ser.convg.to IE_{ad}=13.20 eV[b]			
$1b_1 \rightarrow$ 3 s (δ= −0.004)			
9.792	78,978	1.996	*(78,989)*[c]
Rydb.Ser.convg.to IE_{ad}=14.77 eV[b]			
$4a_1 \rightarrow ns$ ($\bar{\delta}$=1.027)			
11.455	92,633	2.025	–
~13.17	~106,223	~2.92	–
$4a_1 \rightarrow 3p$ (δ=0.42)			
12.73	102,674	2.58	–
Rydb.Ser.convg.to IE_{ad}=15.52 eV[b]			
$2b_2 \rightarrow$ 4 s/3d (δ=0.970/−0.030)			
14.038	113,224	3.03	–

[a] Adiabatic ionization energy as measured in this work (see Section 5.1.1).
[b] Adiabatic ionization energies obtained in this work by quantum chemical calculations.
[c] Data reported by [2] but differing or corresponding to several assignments are listed in *italic* and in parentheses.
[d] Data listed in square brackets correspond to at least two possible assignments (see text) in the present work.

Table 2
Calculated wavenumbers (cm^{-1}) for the neutral $\tilde{X}^1A_1$ and 3^1B_2 states at M02–6X level and the 4^1A_1, 6^1B_1 and 7^1A_1 states at the TDDFT/M02–6X level. No scaling factor is applied to the calculated values. For the neutral ground state comparison is made with experimental data [16].

States	$\tilde{X}^1A_1$		3^1B_2	4^1A_1	6^1B_1	7^1A_1
Modes	Exp [16]	M06–2X	M02–6X	TDDFT	TDDFT	TDDFT
a_1						
ν_1	3023	3175	3152	3190	3208	3173
ν_2	1593	1688	1674	1407	1639	1623
ν_3	1279	1389	1278	1213	1411	1359
ν_4	467	497	298	471	796	243
ν_5	184	196	144	197	**i589**	110
a_2						
ν_6	696	675	526	**i879**	358	635
b_1						
ν_7	886	938	849	575	1025	915
ν_8	405	435	**i220**	485	547	217
b_2						
ν_9	3108	3280	3255	3321	**7952 !**[a]	3274
ν_{10}	1049	1081	775	1079	1264	2388
ν_{11}	668	732	294	822	820	831
ν_{12}	322	331	**i287**	251	576	233

[a] For explanation see text.

Table 3
(a) Vertical and/or adiabatic excitation energies (eV) of neutral states of 1,1-$C_2H_2Br_2$ obtained at the TDDFT level. The calculations were carried out with the aug-cc-pVDZ basis set. (b) Structure and assignment for the 6^1B_1 Rydberg state. Conversion factor: 1 eV= 8 065.545 eV [11].

(a)

E_{vert}(eV)	E_{ad}(eV)	Description	
5.90	4.71	$n_\sigma \rightarrow$Rs: $\mathbf{3^1B_2}$ (CP2)	
6.17	5.77	$\pi+n_\pi \rightarrow \pi^*$: $\mathbf{4^1A_1}$ (TS)	
6.51	6.33	$\pi+n_\pi \rightarrow$ Rs: $\mathbf{6^1B_1}$ (TS)	
6.55	5.16	$n_\sigma \rightarrow 3s$	$\mathbf{7^1A_1}$
		$n_\sigma \rightarrow 3p_y, 3d_{yz}$	
7.12	-	$n_\pi \rightarrow \pi^*$: $\mathbf{9^1B_2}$	
7.42	-	$\pi+n_\pi \rightarrow 3p_z$: $\mathbf{12^1B_1}$	

(b)

eV	cm^{-1}	Assignment
6.583	53,095	$\mathbf{6^1B_1(0,0)}$
6.651	53,644	$\nu_8(\nu_{12})$
6.688	53,942	na
6.713	54,144	$2\nu_8(2\nu_{12})$
6.750	54,442	$\boldsymbol{\nu_3}$
6.818	54,991	$\nu_3+\nu_8(\nu_{12})$

CP2: second order critical point. TS: transition state.

at DFT/M06–2X/aug-cc-pVDZ level are represented in Fig. S2 (see Supplementary material).

4.2. Calculation results

4.2.1. The neutral states (Fig. S2a-b)

Only the optimized geometry in the C_{2v} symmetry point group for the neutral $\tilde{X}^1A_1$ state and a few allowed excited states are listed in Table S1 (see Supplementary material). The geometry optimization of the 3^1B_2 and the 4^1A_1 don't converge. The former leads to dissociation by atomic Br-loss. The latter shows a major lengthening of the C=C bond and a shortening of the C-Br bond.

It has to be pointed out that the planar 4^1A_1 (see Fig. S2a) state optimized in the C_{2v} point group evolves into a transition state (TS) and no minimum could be determined. The geometry optimization without constraints of this transition state leads to a lower energetic and non-planar state of C_{2v} symmetry: the CH_2-group is in a plane at 90° to that containing CBr_2. This geometry corresponds to a second order critical point state with two imaginary wavenumbers.

The 7^1A_1 state is the only allowed excited state showing a minimum in the C_{2v} symmetry point group. It shows a nearly as large C-Br internuclear distance (2.1144 Å) as the 4^1A_1 state (1.8308 Å).

Table 2 shows the wavenumber calculation results for the neutral ground and several neutral excited states. Only those results obtained for the $\tilde{X}^1A_1$ ground state could be compared to Raman spectroscopic data obtained by de Hemptinne et al. [16].

The 6^1B_1 transition state (see Fig. S2b) is remarkable showing an imaginary wavenumber of a_1 representation. This is probably related to the abnormally high ν_9 (b_2) wavenumber of 7952 cm^{-1} likely to be linked with a coupling of this state with the closely lower-lying but forbidden 5^1A_2 state.

The vertical and/or adiabatic excitation energies calculated in the C_{2v} point group for several neutral states are listed in Table 3a. True adiabatic excitation energy has only been obtained for the 7^1A_1 state. The optimized geometry in the C_{2v} symmetry point group not being a minimum even at lower symmetry, the other values are only indicative.

4.2.2. The ionized states (Fig. S2 c-e)

The optimized geometry was calculated at the M02–6X level for the $\tilde{X}^2B_1$, $\tilde{A}^2B_2$, $\tilde{B}^2A_2$ and $\tilde{C}^2A_1$ states and at the TDDFT level for the other states. Table 4 displays the calculated adiabatic (IE_{ad}) and/or vertical (IE_{vert}) ionization energies characterizing the successive ionic states. Comparison is made with previous experimental HeI- [3] and HeII-PES [4] results.

It has to be noticed that above the $\tilde{E}^2B_1$ state, doubly excited configuration states occur. The $\tilde{G}^2B_2$ and $\tilde{H}^2B_2$ arise from the ionization of the same $2b_2$ molecular orbital (MO) together with a mixture of configuration interaction. The same remark is valid for the $\tilde{I}^2A_1$ and $\tilde{J}^2A_1$ (IE_{vert}=18.16 eV and 18.29 eV), not included in Table 4, and involving the $3a_1$ MO ionization.

The wavenumbers for the twelve vibrational coordinates of 1,1-$C_2H_2Br_2^+$ have been calculated for the $\tilde{X}^2B_1$ to the $\tilde{H}^2B_2$ ionic states. Only the results concerning $\tilde{X}^2B_1$ to the $\tilde{F}^2A_1$ states are listed in Table 5. No scaling factor has been applied.

5. Discussion

5.1. The (Dissociative) photoionization of 1,1-$C_2H_2Br_2^+$

The photoionization mass spectrum of 1,1-$C_2H_2Br_2$ recorded at $h\nu$=20 eV is essentially composed of a broad peak centered on m/e = 186 corresponding to the combinations of the two isotopic species of 1,1-C_2H_2 $^{79,81}Br_2^+$ and a narrower peak at m/e = 106 containing the two isotopic components of $C_2H_2{}^{79,81}Br^+$. Their absolute intensities are 46.9% and 49.2% respectively. Two very weak signals are observed at m/e = 80 (Br^+) and m/e = 160 (Br_2^+) representing each an intensity of 1.2% and 1.7%. These abundances are close to those observed for the same ions in the mass spectrum obtained by 20 eV electron impact on the cis- and trans-$C_2H_2Br_2$ isomers [17].

5.1.1. The photoionization efficiency of 1,1-$C_2H_2Br_2^+$ (Figs. 3 and 4)

The photoionization efficiency curve (PIEC) of 1,1-$C_2H_2Br_2^+$ up to 15 eV is displayed in Fig. 3 and has been recorded with 5 meV energy increments. As mentioned in Table 4 the photoelectron spectroscopic studies [3,4] reported only the vertical ionization energies (IE_{vert}). However, the knowledge of their adiabatic value (IE_{ad}) will be important for the analysis of the vacuum UV-PAS of 1,1-$C_2H_2Br_2$ (see Section 5.2). Therefore the IE_{ad} values have been determined by *ab initio* calculations. The results are listed in Table 4 for the successive ionic states. It has to be noticed that, for the $\tilde{B}^2A_2$ and $\tilde{C}^2A_1$ states, $IE_{ad} \approx IE_{vert}$.

The PIEC of 1,1-$C_2H_2Br_2^+$ near threshold is reproduced on an expanded photon energy scale in Fig. 4 together with the PAS mea-

Table 4
Vertical and adiabatic ionization energies (eV) determined at two calculation levels for the cationic states resulting from direct MO ionization. Previous HeI-PES [3] and HeII-PES [4] results are included.

Ion State	$\tilde{X}^2B_1$		$\tilde{A}^2B_2$		$\tilde{B}^2A_2$		$\tilde{C}^2A_1$	
Level	IE_{vert}	IE_{ad}	IE_{vert}	IE_{ad}	IE_{vert}	IE_{ad}	IE_{vert}	IE_{ad}
UM06–2X	9.76	9.54	10.83	10.52	11.24	11.24	11.69	11.63
TDDFT	9.76	9.54	10.75	–	11.54	–	11.59	–
This work	9.778	9.617	–	–	–	–	–	–
[3]	9.78	–	10.73	–	11.23	–	11.60	–
[4]	9.78	–	10.73	–	11.2	–	11.6	–
	$\tilde{D}^2B_2$		$\tilde{E}^2B_1$		$\tilde{F}^2A_1$		$[\tilde{H},\tilde{G}]^2B_2$ [a]	
TDDFT	13.06	12.77	13.44	13.2	15.21	14.77	15.85	14.97
[3]	13.0	–	13.0	–	15.20	–	15.90	–
[4]	~13	–	13.3	–	15.2	–	16.0	–

[a] see text in Sections 4.2.2 and 5.2.3.

Table 5
Calculated wavenumbers (cm^{-1}) for the first seven ionized states of 1,1-$C_2H_2Br_2$ at the M02–6X level. No scaling factor is applied to the calculated values.

State	$\tilde{X}^2B_1$	$\tilde{A}^2B_2$	$\tilde{B}^2A_2$	$\tilde{C}^2A_1$	$\tilde{D}^2B_2$	$\tilde{E}^2B_1$	$\tilde{F}^2A_1$
a_1							
ν_1^+	3180	3160	3165	3176	2885	3142	2858
ν_2^+	1495	1721	1688	1579	1797	1619	1453
ν_3^+	1349	1376	1389	1420	834	1383	1115
ν_4^+	522	505	485	432	372	402	422
ν_5^+	212	185	186	202	177	164	152
a_2							
ν_6^+	351	661	674	659	493	686	613
b_1							
ν_7^+	1000	977	992	988	694	966	865
ν_8^+	442	339	386	400	398	369	297
b_2							
ν_9^+	3305	3265	3269	3282	2675	3261	3280
ν_{10}^+	1140	977	1005	1125	879	1140	1663
ν_{11}^+	823	606	546	672	431	757	734
ν_{12}^+	324	275	317	318	274	293	330

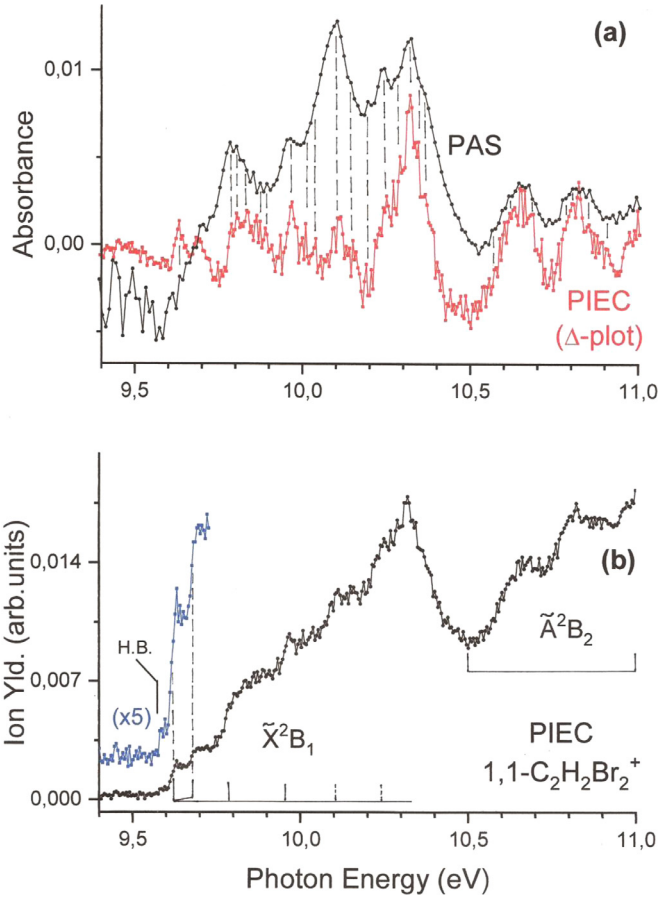

Fig. 4. (a) VUV photoabsorption spectrum (PAS) (black) of 1,1-$C_2H_2Br_2$ and Δ-plot (red) of the (b) photoionization efficiency curve (PIEC) of 1,1-$C_2H_2Br_2^+$ on an expanded energy scale between 9.4 eV and 11.0 eV. Vertical bars indicate the band maxima corresponding to autoionization in the PAS and critical energies and Franck-Condon regions in the PIEC. H.B. corresponds to a hot band.

sured in the same photon energy range. Marked by vertical bars many correspondences between the two spectra are obvious. In the energy range of 9.6 eV three onsets have been observed, i.e. at 9.579 eV, 9.617 eV and 9.677 eV successively.

The threshold at 9.617±0.005 eV is assigned to the $IE_{ad}(\tilde{X}^2B_1)$ state of 1,1-$C_2H_2Br_2$. This value is in agreement with 9.54 eV obtained in the present work by quantum chemical calculations. The weak signal measured at 9.579 eV, i.e. 38±10 meV (306±80 cm^{-1}) below $IE_{ad}(\tilde{X}^2B_1)$ could be assigned to the ionization of vibrationally hot 1,1-$C_2H_2Br_2$. This energy difference could correspond to the vibrational excitation of $\nu_4(a_1)$=467 cm^{-1} or more likely to $\nu_{12}(b_2)$=322 cm^{-1} [16]. The relative intensity ratio of about 25% observed for these two transitions is comparable to the calculated Boltzmann factors of 11% and 21%. The present IE_{ad} could only be compared to, but is higher than, the equivalent value measured by photoionization for the cis- and trans-1,2-$C_2H_2Br_2$ isomers [17], i.e. 9.45±0.01 eV (*cis*) and 9.46±0.01 eV (trans). The same trend has been observed for the three corresponding dichloroethylene isomers [18].

The onset at 9.677 eV is at 60±10 meV (480±40 cm^{-1}) above $IE_{ad}(\tilde{X}^2B_1)$. By quantum chemical calculations two wavenumbers of the molecular ion could correspond to this experimental value: $\nu_4^+(a_1)$=522 cm^{-1} and $\nu_8^+(b_1)$=442 cm^{-1} The observed intensity of this transition would favor the former assignment.

Figure 4b shows a series of "steps" at 9.778 eV, about 9.85 eV and 9.953 eV and intensity increases near 10.085 eV and 10.220 eV successively. For the first and third critical points energy differences of 0.161±0.010 eV and 0.336±0.010 eV (or 2 × 0.168 eV) are measured with respect to the threshold at IE_{ad}=9.617 eV. The average energy interval is 0.166±0.005 eV corresponding to a wavenumber of 1336±40 cm^{-1}. By quantum chemical calculations this quantity corresponds to ν_3^+=1349 cm^{-1} involving the C = C stretching and CH_2 bending vibration. The intensity increase at 9.778 eV should correspond to the $IE_{vert}(\tilde{X}^2B_1)$ which is in agreement with the HeI- and HeII-PES values of 9.78 eV [3,4]. By quantum chemical calculations 9.76 eV is obtained. The intermediate energy at about 9.85 eV has probably to be assigned to the com-

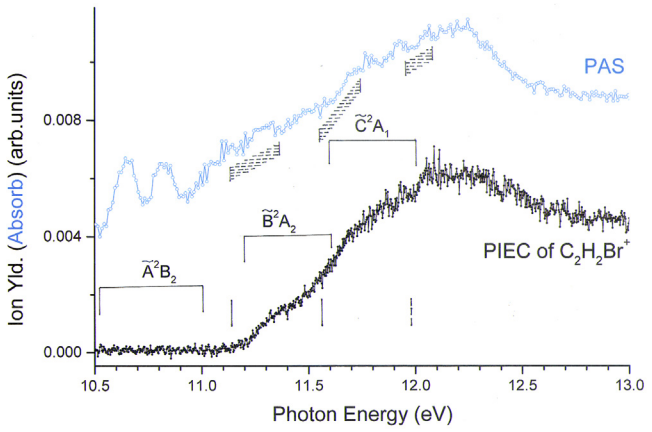

Fig. 5. VUV photoabsorption (PAS) of 1,1-$C_2H_2Br_2$ and photoionization efficiency curve (PIEC) of $C_2H_2Br^+$ between 10.5 eV and 13.0 eV. The Franck-Condon regions of the ionic states are indicated. Long vertical bars locate the critical energies. Shaded areas cover the absorption regions corresponding to $C_2H_2Br^+$ ion yield.

bined excitation of $\nu_3^+ + \nu_4^+$. The following two onsets are less accurate owing to stronger autoionization contribution. They could likely be assigned to the continuation of the ν_3^+ vibrational progression but involving anharmonicity. The considered autoionizing states will be analyzed and identified in Section 5.2.

Above 10.5 eV the PIEC of 1,1-$C_2H_2Br_2^+$ clearly shows two relatively strong step-like increases at 10.592 eV and 10.772 eV which are both clearly correlated with autoionization of Rydberg states occurring at the same energy (see Fig. 4a). In the HeI(HeII)-PES [3,4] $IE_{vert}(\tilde{A}^2B_2)$=10.73 eV. This value is in good agreement with that calculated in the present work at 10.83 eV. The calculated $IE_{ad}(\tilde{A}^2B_2)$=10.52 eV is close to the experimental value at 10.592 eV. However, this latter value corresponds to the inflexion point of the sigmoïdal ion intensity curve extending between 10.5–10.7 eV. Actually the ion current rises up from about 10.54 eV. The slowness of the PIEC's rise could likely be due to an unresolved vibrational progression involving e.g. ν_5^+=185 cm^{-1} (0.023 eV) (CBr_2 bending). As shown in Table S2 the C = C bond length is appreciably shortened and the Br-C = C angle is strongly opened in the $\tilde{A}^2B_2$ ionic state.

As shown in Fig. 3 no critical energy is observed in the energy range of the ionic $\tilde{B}^2A_2$ state. Up from 11.6 eV to 13.2 eV a broad and strong peak dominates the PIEC of 1,1-$C_2H_2Br_2^+$. It correlates unambiguously with a strong broad absorption band present in the PAS and will be described and assigned in Section 5.2. In this energy range the $\tilde{C}^2A_1$ ionic state has been observed by HeI(HeII)-PES [3,4]. It has to be stressed that for both the $\tilde{B}^2A_2$ and $\tilde{C}^2A_1$ states $IE_{vert} \approx IE_{ad}$ and calculated at 11.24 eV and 11.63 eV respectively. These results have to be compared with the experimental PES values of 11.23 eV [3] and 11.60 eV [3] respectively.

Above 13.2 eV the PIEC is almost flat up to 13.8 eV where it shows a broad weak band which is also connected with neutral states observed in the PAS. In this energy range the doublet PES band $\tilde{D}^2B_2$-$\tilde{E}^2B_1$ has been reported [3,4]. By quantum chemical calculations IE_{ad}= 12.77 eV and 13.2 eV and the corresponding IE_{vert}=13.06 eV and 13.44 eV were obtained. These latter calculated values have to be compared with the experimental values reported at 13.0 eV [3] and 13.3 eV [3,4].

5.1.2. The photoionization efficiency of $C_2H_2Br^+$ (Figs. 3 and 5)

The PIEC of the $C_2H_2Br^+$ fragment ion is reproduced in Fig. 5 between 10.5 eV and 13.0 eV. The PAS of 1,1-$C_2H_2Br_2$ observed in the same photon energy range is included in the same figure. Essentially three slope changes are observed i.e. at 11.14±0.02 eV, 11.56±0.01 eV and 11.98±0.01 eV successively. As clearly shown in Fig. 5 the first two dissociative ionization processes take place in the energy range of (i) the $\tilde{B}^2A_2$ and $\tilde{C}^2A_1$ ionic states and of (ii) neutral states observed in the PAS.

The lowest threshold determined for the appearance of $C_2H_2Br^+$ has most likely to be assigned to:

$$1,1-C_2H_2Br_2 + h\nu \rightarrow C_2H_2Br^+(\tilde{X}^1A_1) + Br(^2P_{3/2}) + e^- \quad (1)$$

provided each fragment being produced in its ground electronic (and vibrational) state carrying no translational kinetic energy. Under these conditions and from reaction (1) a value of the dissociation energy $D(H_2CCBr^+\text{-}Br)$=1.52±0.03 eV could be derived.

The next threshold observed in the PIEC of $C_2H_2Br^+$ is located at 0.42±0.03 eV above the lowest onset and has very likely to be assigned to the reaction:

$$1,1-C_2H_2Br_2 + h\nu \rightarrow C_2H_2Br^+(\tilde{X}^1A_1) + Br(^2P_{1/2}) + e^- \quad (2)$$

where the energy separation of 0.42±0.03 eV has very likely to be assigned to the $^2P_{3/2}$–$^2P_{1/2}$ spin-orbit splitting of 3685 cm^{-1} or 0.457 eV as determined by atomic spectroscopy [19].

The autoionization of neutral states observed between 11.6 eV and 13.2 eV leads to the production of both $C_2H_2Br_2^+$ and $C_2H_2Br^+$. Likely the sudden increase of the $C_2H_2Br^+$ ion yield at 11.98 eV corresponds to:

$$1,1-C_2H_2Br_2 + h\nu \rightarrow C_2H_2Br^+(^3A_2) + Br(^2P_{3/2}) + e^- \quad (3)$$

where the 0.84 eV excess energy could be assigned to the electronic excitation of the $C_2H_2Br^+$fragment ion. A $^3A_2$ excited state was calculated for $C_2H_2F^+$ at 2.52 eV above the ground state [20].

Similarly and above 13.4 eV autoionization plays a major role in the production of $C_2H_2Br^+$ as it does for $C_2H_2Br_2^+$. The absence of ionization cross-section in the 13.9–14.9 eV energy range of the HeI-PES [3] and in the HeII-PES [4] corroborates this analysis.

5.2. The vacuum UV-PAS of 1,1-$C_2H_2Br_2$

As mentioned in Section 5.1 in the mass spectrum of 1,1-$C_2H_2Br_2$, recorded at 20 eV signals corresponding to $Br_2^+$and Br^+ have been detected. To be aware of any suspicious contribution of molecular Br_2 or atomic Br to the 1,1-$C_2H_2Br_2$ vacuum UV PAS we recorded the vacuum UV PAS of Br_2 [21] or referred to the atomic spectrum of Br [22]. The comparison bore no evidence for Br_2 or Br absorptions particularly in the high absorbance regions of these species in the 7.5–8.35 eV, 8.44–8.71 eV and 9.4–9.78 eV regions.

The simplest model for the Rydberg series analysis consists to neglect the perturbations due to Rydberg-Rydberg interactions. To fit their position (E_{Ryd}) the Rydberg formula (1)

$$E_{Ryd} = IE - R/(n-\delta)^2 = IE - R/(n*)^2 \quad (4)$$

has been used. R is the Rydberg constant R = 13.6057 eV [11], δ is the quantum defect, n* is the effective quantum number and IE is the convergence limit or ionization energy of the considered Rydberg series. The successive ionization energies IE used in this work were defined in Table 3 and are inserted in Figs. 1 and 2. IE_{ad} has been adopted for excitations where the (0,0) vibrational transition has been identified. Otherwise, the IE_{vert} has been chosen as the convergence limit.

5.2.1. The transitions between 5.6 eV and 6.9 eV (see Figs. 1 and 6a)

The typical broad band observed at low energy in the vacuum UV PAS of the ethylene compounds has its maximum at 6.231 eV (50,256 cm^{-1}) in 1,1-$C_2H_2Br_2$ and is shown in Fig. 1. Fig. 6a shows the band on expanded energy scale and where the red curve in the upper part of the figure represents the continuum to be subtracted from the original signal. The resulting Δ-plot displayed in the lower part of Fig. 6a clearly shows three well separated parts: (a) a broad doublet, (b) a more complex structured part consisting

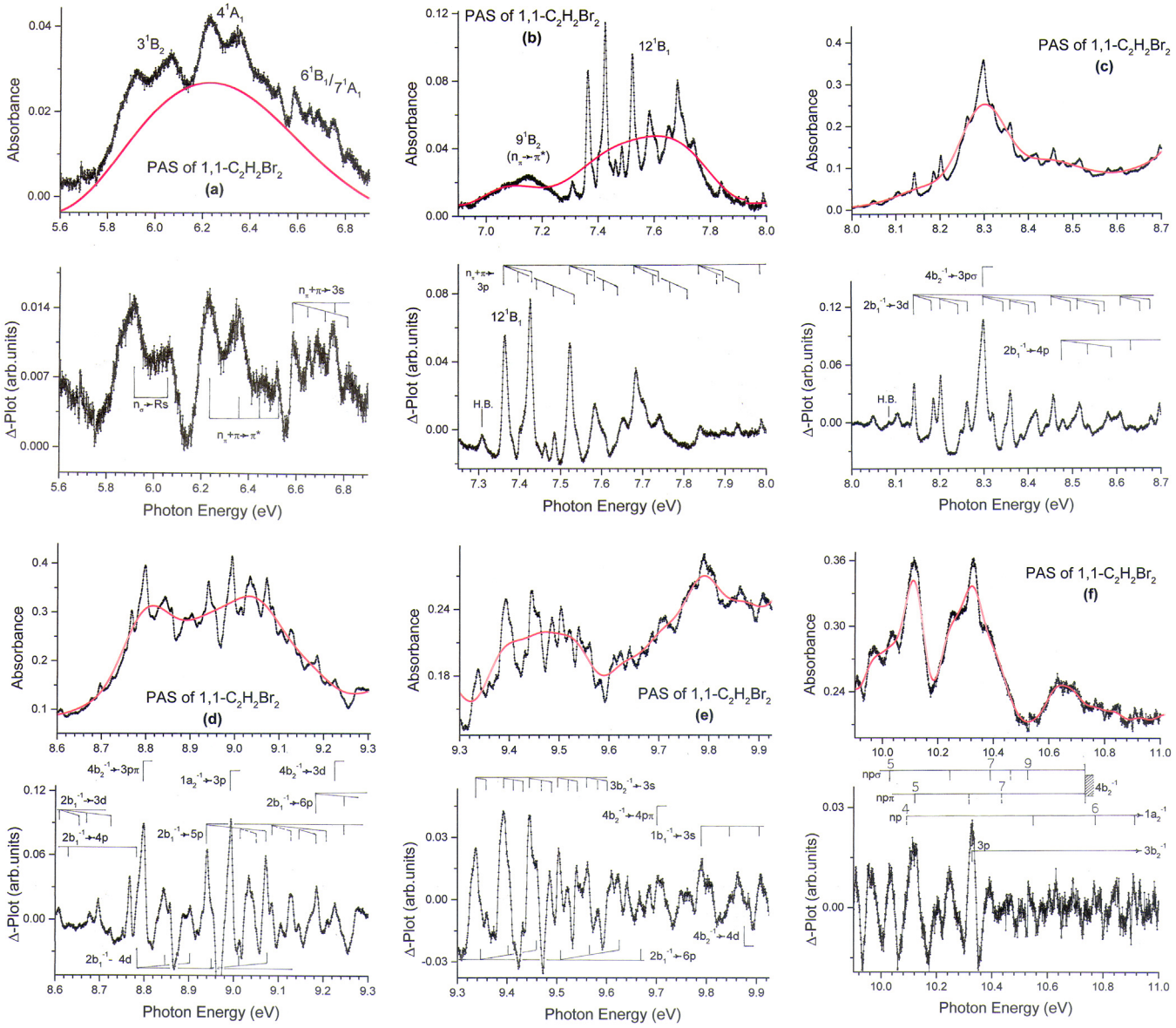

Fig. 6. VUV photoabsorption spectrum of 1,1-$C_2H_2Br_2$ on an expanded photon energy scale between 5.0 eV and 11.0 eV. The upper and lower panels show the absorbance and the corresponding Δ-plot respectively for (a) 5.6–6.9 eV, (b) 6.9–8.0 eV, (c) 8.0–8.7 eV, (d) 8.6–9.3 eV, (e) 9.3–9.9 eV and (f) 9.9–11.0 eV. The red curve in the upper panels corresponds to the continuum used for subtraction leading to the Δ-plot. Long vertical bars locate the vibrationless (0,0) transitions of the indicated Rydberg transitions. For each transition the progression(s) is (are) drawn by short vertical bars.

of at least four broad peaks and (c) the beginning of a series of narrower peaks extending up from 6.6 eV to 6.9 eV.

For the assignment of the features observed in this energy region quantum chemical calculations have been performed. Several neutral states have been calculated at the C_{2v} symmetry point group between 5.1 eV and 7.5 eV. Their optimized geometry and vibrational wavenumbers were obtained. Only those allowed to be reached from the $\tilde{X}^1A_1$ neutral ground state are listed in Table S1 and Table 3a where the corresponding excitation energies are also displayed.

The strongest transition is calculated for the 4^1A_1 state corresponding to the $\pi(+n_\pi)\rightarrow\pi^*$ excitation with $E_{exc}{}^{ad}$=5.77 eV and $E_{exc}{}^{vert}$=6.17 eV. This state is a transition state involving a virtual b_1 MO containing Rydberg p character and could likely be assigned to the features observed between 6.231 eV and 6.516 eV. The broad width of the peaks is probably related to the life time of the vibronic states. The interval between the first three peaks at 6.231 eV, 6.344 eV and 6.458 eV is about 0.114 eV (911 cm^{-1}) and between 6.344 eV and 6.516 eV a difference of 0.172 eV (1378 cm^{-1}) is measured. This latter value would be comparable to ν_2=1407 cm^{-1} calculated for 4^1A_1. These intervals are also close to those observed in the first band of the HeI-PES of 1,1-$C_2H_2Br_2$ [3]. Schander and Russell [2] mention a pair of bands at 50,350 cm^{-1} (6.242 eV) and 51,230 cm^{-1} (6.352 eV). These authors invoked the possible but forbidden $2b_2(\pi)\rightarrow b_1(\sigma^*)$ transition.

At 6.583 eV (53,095 cm^{-1}) a sharply rising peak is observed and followed by several narrow features listed in Table 3b. This energy is close to the excitation energy predicted for the 6^1B_1 and the 7^1A_1 states, $E_{exc}{}^{vert}$= 6.51 eV and 6.55 eV respectively. Assuming the experimental $E_{exc}{}^{ad}$= 6.583 eV the 6^1B_1 state should be involved as predicted $E_{exc}{}^{ad}$=6.33 eV and corresponding to the $\pi(2b_1)\rightarrow$3 s Rydberg transition. It should be characterized by n^*=2.118 and δ=0.882. Schander and Russell [2] determined a Rydberg series starting at 53,129 cm^{-1}. The following structure should be assigned to vibrational excitation. Table 3b suggests a possible interpretation involving $\nu_3(a_1)$ =1347 cm^{-1} (0.167 eV) and $\nu_8(b_1)$

(or $\nu_{12}(b_2)$)=530 cm^{-1} (0.066 eV). These values have to be compared with those predicted at 1411 cm^{-1} and 547 (576) cm^{-1} respectively.

At the low energy side of the broad peak at 6.231 eV a doublet feature is observed at 5.911 eV (47,675 cm^{-1}) made of two broad peaks separated by 0.146 eV (1177 cm^{-1}). A weak shoulder is measured at 5.80 eV. Schander and Russell [2] mention a pair of peaks at 47,820 cm^{-1} and 49,020 cm^{-1}. From the present calculations a transition to the 3^1B_2 state is allowed and appears at $E_{exc}{}^{vert}$=5.90 eV and $E_{exc}{}^{ad}$=4.71 eV. However, this state is a second-order critical state showing very large C-Br internuclear distances (up to 2.26 Å) and Br-C = C bond angles (up to 140°). Conceivably, the interval of 1177 cm^{-1} could be assigned to $\nu_3(a_1)$(C = C stretch) predicted at 1278 cm^{-1}.

Finally, a weaker broad band is measured at 7.15 eV (57,669 cm^{-1}) (see Fig. 6b). This observation could likely be accounted for by the allowed transition to the 9^1B_2 excited state calculated at $E_{exc}{}^{vert}$= 7.12 eV and assigned to a $n_\pi \rightarrow \pi^*$ transition. This interpretation has also been proposed by Schander and Russell [2].

5.2.2. Rydberg transitions between 7.3 eV and 11.0 eV (see Figs. 1 and 6b-f)

The vibrationless Rydberg transitions observed for 1,1-$C_2H_2Br_2$ between 7.3 eV and 11 eV are shown in Fig. 1 and have been listed in Table 1 together with their effective quantum numbers. In the same Table the previous dataset reported by Schander and Russell [2] is included for comparison. For the assignments reported in the present work the adiabatic ionization energy value IE_{ad}(1,1-$C_2H_2Br_2{}^+$,$\tilde{X}^2B_1$) = (9.617±0.005) eV has been adopted whereas the value used by Schander and Russell [2] was 9.78 eV actually corresponding to the $IE_{vert}(\tilde{X}^2B_1)$.

For the first three excited states of the ion, i.e. $\tilde{A}^2B_2$, $\tilde{B}^2A_2$ and $\tilde{C}^2A_1$, the IE_{vert} values measured by HeI- [3] and HeII-PES [4] have been adopted. It has to be kept in mind that IE_{ad}=IE_{vert} for the latter two states only. For the $\tilde{A}^2B_2$, the theoretical calculations provide IE_{ad}=10.52 eV whereas IE_{vert}=10.83 (10.75) eV. The four excited states observed up to 16 eV are all characterized by their IE_{vert} only [3,4]. The quantum chemical calculations presented in the present work yield also the IE_{ad} and these values will be used as convergence limit in the forthcoming section.

5.2.2.1. Rydberg series converging to $\tilde{X}^2B_1$ at 9.617 eV. Short $\pi(2b_1)\rightarrow$np (n = 3–6) and $\pi(2b_1)\rightarrow$nd (n = 3, 4) Rydberg series are observed. They are characterized by δ=0.55±0.02 and −0.04±0.01 respectively. For both series more or less long vibrational progressions have been measured and their components have been indexed in Table 6. A particularly well-developed and isolated progression is observed for the $2b_1\rightarrow$3p and the $2b_1\rightarrow$3d Rydberg transitions at 7.364 (59,395 cm^{-1}) and 8.142 eV (65,670 cm^{-1}). The transition energy measured for the former Rydberg state corresponds fairly well to 7.42 eV predicted by quantum chemical calculations in the present work and designated by 12^1B_1.

For the $2b_1\rightarrow$3p Rydberg transition the assignment of the successive features are inserted in Table 6. From these data several wavenumbers are deduced: $\omega_4(\omega_8)$= 476±50 cm^{-1} (59±6 meV), ω_5=145±8 cm^{-1} (18±1 meV) and $\omega_6(\omega_{12})$= 371±16 cm^{-1} (46±2 meV). A last value has been obtained by plotting the IE_{vib} versus the assigned vibrational quantum number "v" as shown in Fig. 7a providing an extrapolated value $\omega_3{}^{ex}$= 1315±16 cm^{-1} (163±2 meV) and the anharmonicity $\omega_{3\times3}$= 6.4 ± 2.4 cm^{-1} (0.8 ± 0.3 meV).

The convergence limit of the considered Rydberg state being the $\tilde{X}^2B_1$ state, the shape and the structure of the corresponding PAS band are expected to be close to the HeI-PES band. By quantum chemical calculations $\nu_3{}^+(a_1)$=1349 cm^{-1}, $\nu_4{}^+(a_1)$=522 cm^{-1}, $\nu_8{}^+(b_1)$=442 cm^{-1}, $\nu_5{}^+(a_1)$=212 cm^{-1}, $\nu_6{}^+(a_2)$=351 cm^{-1}

Table 6
Energy position (eV), wavenumber (cm^{-1}) and assignments proposed for the vibrational structure of Rydberg states observed in the vacuum UV photoabsorption spectrum of 1,1-$C_2H_2Br_2$ between 7.3 eV and 9.7 eV and converging to the $\tilde{X}^2B_1$ ionic ground state. Conversion factor 1 eV=8 065.545 cm^{-1} [11].

This work			
Energy (eV)	Wavenbr. (cm-1)	Assignment	
$2b_1\rightarrow$3p (12^1B_1)			
7.310	58,959	HB	$\omega_3{}^{ex}$=163±2 meV[a]
7.364	59,395	**(0,0)**	1315±16 cm^{-1}
7.381	59,532	ν_5	$\omega_{3\times3}$=0.8 ± 0.3 meV
7.401	59,693	$2\nu_5$	6.4 ± 0.2 cm^{-1}
7.412	59,782	$\nu_6(\nu_{12})$	ω_4=59±6 meV
7.425	59,887	$\nu_4(\nu_8)$	476±50 cm^{-1}
7.443	60,032	$\nu_4+\nu_5$	ω_5=18±1 meV
7.461	60,177	$2\nu_6(2\nu_{12})$	145±8 cm^{-1}
7.484	60,362	$2\nu_4(2\nu_8)$	ω_6=46±2 meV
7.510	60,572	$3\nu_6(3\nu_{12})$	371±16 cm^{-1}
7.522	60,669	$\boldsymbol{\nu_3}$	
7.538	60,798	$3\nu_4(3\nu_8)/\nu_3+\nu_5$	
7.566	61,024	$\nu_3+\nu_6(\nu_{12})$	
7.583	61,161	$\nu_3+\nu_4(\nu_8)$	
7.608	61,362	$\nu_3+2\nu_6(2\nu_{12})$	
7.631	61,548	$\nu_3+\nu_4(\nu_8)+\nu_6(\nu_{12})$	
7.652	61,717	na	
7.671	61,870	na	
7.683	61,968	$\boldsymbol{2\nu_3}$	
7.701	62,113	$2\nu_3+\nu_5$	
7.715	62,226	na	
7.726	62,314	$2\nu_3+\nu_6(\nu_{12})$	
7.741	62,435	$2\nu_3+\nu_4(\nu_8)$	
7.797	62,887	$2\nu_3+2\nu_4(2\nu_8)$	
7.839	63,226	$\boldsymbol{3\nu_3}$	
7.895	63,677	$3\nu_3+\nu_4(\nu_8)$	
7.928	63,944	$3\nu_3+2\nu_6(\nu_{12})$	
7.988	64,427	$\boldsymbol{4\nu_3}$	
$2b_1\rightarrow$3d			
8.142	65,670	**(0,0)**	$\omega_3{}^{ex}$=161±2 meV[a]
8.167	65,871	ν_5	1298±16 cm^{-1}
8.185	66,016	$\nu_6(\nu_{12})$	$\omega_{3\times3}$=1.0 ± 0.7 meV
8.202	66,154	$\nu_4(\nu_8)$	8 ± 5 cm^{-1}
8.247	66,516	$\nu_4(\nu_8)+\nu_6(\nu_{12})$	ω_4=60±2 meV
8.261	66,629	$2\nu_4(2\nu_8)$	484±16 cm^{-1}
[8.300][c]	66,944	$\boldsymbol{\nu_3}$	ω_5=18±3 meV
8.318	67,089	$\nu_3+\nu_5$	145±24 cm^{-1}
8.348	67,331	$\nu_3+\nu_6(\nu_{12})$	ω_6=44±3 meV
8.360	67,428	$\nu_3+\nu_4(\nu_8)$	355±24 cm^{-1}
8.408	67,815	$\nu_3+\nu_4(\nu_8)+\nu_6(\nu_{12})$	
8.418	67,896	$\nu_3+2\nu_4(2\nu_8)$	
8.457	68,210	$\boldsymbol{2\nu_3}$	
8.479	68,388	$2\nu_3+\nu_5$	
8.500	68,557	$2\nu_3+\nu_6(\nu_{12})$	
8.515	68,678	$2\nu_3+\nu_4(\nu_8)$	
8.580	69,202	$2\nu_3+2\nu_4(2\nu_8)$	
8.607	69,420	$\boldsymbol{3\nu_3}$	
8.656	69,815	$3\nu_3+\nu_6(\nu_{12})$	
8.677	69,985	$3\nu_3+\nu_4(\nu_8)$	
8.768	70,864	$\boldsymbol{4\nu_3}$	
$2b_1\rightarrow$4p			
8.479	68,557	**(0,0)**	$\omega_3{}^{av}$=155±4 meV[b]
8.534	68,831	$\nu_4(\nu_8)$	1250±30 cm^{-1}
8.595	69,323	$2\nu_4(2\nu_8)$	ω_4=58±3 meV
8.630	69,606	$\boldsymbol{\nu_3}$	468±24 cm^{-1}
8.696	70,138	$\nu_3+\nu_4(\nu_8)$	
[8.786][c]	[70,864]	$\boldsymbol{2\nu_3}$	
$2b_1\rightarrow$4d			
[8.786][c]	[70,864]	**(0,0)**	$\omega_3{}^{av}$=159±8 meV[b]
8.843	71,324	$\nu_4(\nu_8)$	1282±64 cm^{-1}
8.902	71,799	$2\nu_4(2\nu_8)$	ω_4=59±1 meV
8.953	72,211	$\boldsymbol{\nu_3}$	476±8 cm^{-1}
9.028	72,816	$\nu_3+\nu_4(\nu_8)$	ω_6=42±2 meV
[9.071][c]	[73,162]	$\nu_3+2\nu_4(2\nu_8)$	339±16 cm^{-1}
9.104	73,429	$\boldsymbol{2\nu_3}$	

(*continued on next page*)

Table 6 (*continued*)

This work			
Energy (eV)	Wavenbr. (cm-1)	Assignment	
$2b_1 \rightarrow 5p$			
8.939	72,098	**(0,0)**	ω_3^{av}=150±10 meV[b]
9.013	72,695	$\nu_4(\nu_8)$	1210±80 cm^{-1}
[9.071][c]	[73,162]	$2\nu_4(2\nu_8)$	ω_4=64±6 meV
9.084	73,267	$\boldsymbol{\nu_3}$	516±48 cm^{-1}
9.127	73,614	$\nu_3+\nu_6(\nu_{12})$	ω_6=42±2 meV
9.145	73,759	$\nu_3+\nu_4(\nu_8)$	339±16 cm^{-1}
[9.185][c]	[74,082]	$\nu_3+\nu_4(\nu_8)+\nu_6(\nu_{12})$	
9.208	74,268	$\nu_3+2\nu_4(2\nu_8)$	
9.235	74,485	$\boldsymbol{2\nu_3}$	
$2b_1 \rightarrow 6p$			
[9.185][c]	[73,162]	**(0,0)**	ω_3^{av}=157±5 meV[b]
9.346	75,381	$\boldsymbol{\nu_3}$	1266±40 cm^{-1}
9.402	75,832	$\nu_3+\nu_4(\nu_8)$	ω_4=59±2 meV
9.460	76,300	$\nu_3+2\nu_4(2\nu_8)$	476±16 cm^{-1}
9.503	76,647	$\boldsymbol{2\nu_3}$	
9.562	77,123	$2\nu_3+\nu_4(\nu_8)$	
9.624	77,623	$2\nu_3+2\nu_4(2\nu_8)$	
9.666	77,961	$\boldsymbol{3\nu_3}$	

[a] ω_3^{ex} stays for the corresponding ω_e value obtained by extrapolation.
[b] ω_3^{av} stays for the corresponding ω_e value obtained by averaging.
[c] Energy positions corresponding to two or more assignments are given in square brackets.

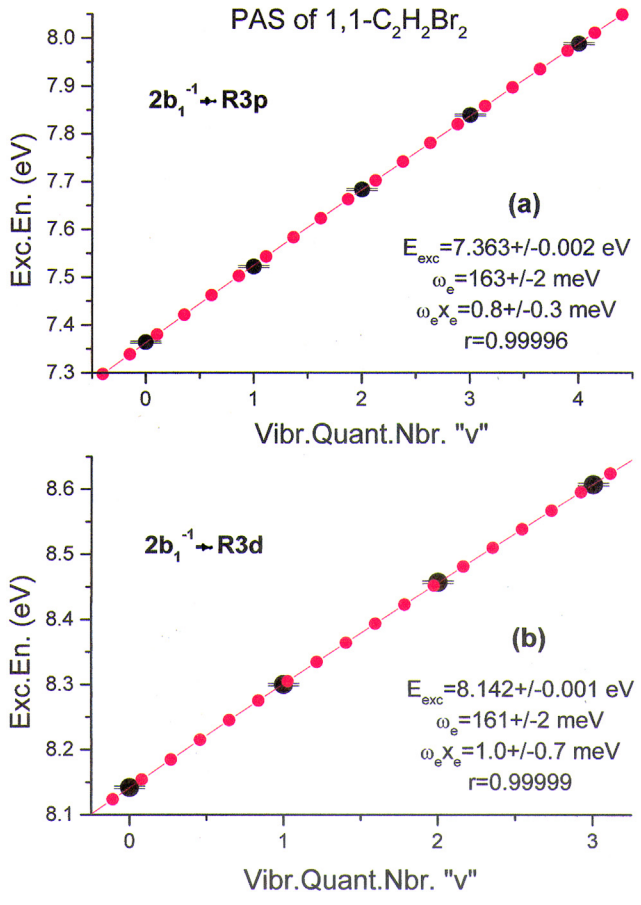

Fig. 7. The excitation energy (eV)-vs-vibrational quantum number v-plot for the (a) $2b_1^{-1} \rightarrow$R3p and (b) $2b_1^{-1} \rightarrow$R3d Rydberg transitions. Experimental values (black points), least square fittings (red points) and fitting parameters are inserted.

and $\nu_{12}^{+}(b_2)$=324 cm^{-1} have been predicted and have to be considered.

Because of the agreement between calculation and experiment the assignment of $\nu_3(a_1)$ and $\nu_5(a_1)$ should be to 1315±16 cm^{-1} and to 145±8 cm^{-1} respectively. Contrarily, the wavenumber of 476±50 cm^{-1} could correspond to both $\nu_4(a_1)$ or $\nu_8(b_1)$. However, the related transitions are strong and therefore to this wavenumber should best correspond the allowed excitation of the $\nu_4(a_1)$ vibrational mode. For the assignment of the wavenumber 371±16 cm^{-1} the $\nu_6(a_2)$ or ν_{12} (b_2) should be considered but are forbidden and should at most appear very weak. However, upon twisting of the molecule these transitions could become allowed.

The above-mentioned results could be compared straightaway to the photoionization results discussed in Section 5.1.1 where two wavenumbers were obtained from the PIEC of 1,1-$C_2H_2Br_2$, i.e. ω_3^{+}= 1336±40 cm^{-1} and ω_4^{+}= 483±40 cm^{-1}.

The values observed in this work can also be compared to those measured in the vacuum UV-PAS reported by Schander and Russell [2], i.e. 1280 cm^{-1} and 490 cm^{-1} assigned to C=C and C-Br stretching vibrations. In their HeI-PES work Wittel and Bock [3] reported wavenumbers of 1200 cm^{-1} and 480cm^{-1}.

As shown in Fig. 6c the $2b_1 \rightarrow 3d$ Rydberg transition also exhibits a long progression (see Table 6). An extrapolated value ω_3^{ex}= 1298±16 cm^{-1} (161±2 meV) and the anharmonicity $\omega_{3\times3}$= 8.0 ± 5.0 cm^{-1} (1.0 ± 0.7 meV) (see Fig. 7b). Other wavenumbers $\omega_4(\omega_8)$= 484±16 cm^{-1} (60±2 meV), ω_5=145±24 cm^{-1} (18±3 meV) and $\omega_6(\omega_{12})$= 355±24 cm^{-1} (44±3 meV) have been measured. These data agree within uncertainty limits with those determined for the $2b_1 \rightarrow 3p$ progression. For the np and nd transitions involving higher n values (see Fig. 6c and d) shorter vibrational progressions are observed and the wavenumbers deduced from these data are listed in Table 6.

5.2.2.2. Rydberg series converging to $\tilde{A}^2B_2$, $\tilde{B}^2A_2$ and $\tilde{C}^2A_1$ at IE_{vert}=10.73 eV and IE_{ad}=11.23 eV and 11.60 eV. The Rydberg transitions involving the $4b_2$-, $1a_2$- and the $5a_1$_MO are related to the lone-pair orbitals mainly centered on the Br atoms. The HeI-PES corresponding to their ionization show fairly narrow bands for the $1a_2^{-1}$ ($\tilde{B}^2A_2$) and $5a_1^{-1}$ ($\tilde{C}^2A_1$) and for which IE_{vert}=IE_{ad} [3,4] as clearly confirmed by the present calculations. The HeI-PES band involving the $4b_2$_MO is broad and symmetric: therefore, it has been characterized by IE_{vert}=10.73 eV [3]. By quantum chemical calculations IE_{ad}=10.52 eV and IE_{vert}=10.83 eV. The large intensity of the absorption bands involving these three transitions is used as a guide for the assignment. Table 1 displays a classification of bands assigned to Rydberg series converging to these three ionic states.

For the $4b_2 \rightarrow n\ell$ Rydberg series no ns-series has been detected. The first series observed are of np-type with two different quantum defects referring to $np\sigma$ and $np\pi$ Rydberg states characterized by $\bar{\delta}_{p\sigma}$=0.636±0.045 and $\bar{\delta}_{p\pi}$=0.330±0.026 respectively. Such series were also observed in the vacuum UV-PAS of 1,1-$C_2H_2Cl_2$ where the energy difference between the first terms was 0.586 eV [23]. This quantity could be compared with the $3p\sigma - 3p\pi$ energy difference measured in the vacuum UV-PAS of 1,1-$C_2H_2Br_2$ and being 0.498 eV. Only two $4b_2 \rightarrow nd$ (n = 3, 4) were identified with $\bar{\delta}$= −0.008±0.002.

For the $1a_2 \rightarrow n\ell$ and $5a_1 \rightarrow n\ell$ Rydberg series only ns- and np-type series have been identified. In both cases the quantum defects are close to the atomic value [25]: δ_s=0.997 and δ_p=0.544 for $1a_2^{-1}$ and δ_s=0.998 and δ_p=0.487 for $5a_1^{-1}$ [25].

5.2.2.3. Rydberg series converging to $\tilde{D}^2B_2$ at IE_{ad}=12.77 eV and $\tilde{E}^2B_1$ at IE_{ad}=13.2 eV. The HeI-PES corresponding to these two ionized states is a broad band extending between 12.5 eV and 13.8 eV and exhibits an unassigned fine structure. Wittel and Bock [3] reported only a maximum at about 13.0 ± 0.2 eV and mentioned

Table 7
Energy position (eV), wavenumber (cm^{-1}) and assignments proposed in the present work for the vibrational structure observed in the vacuum UV photoabsorption spectrum of 1,1-$C_2H_2Br_2$ between 9 eV and 10 eV and converging to $\tilde{D}^2B_2$ and $\tilde{E}^2B_1$ ionized states. Conversion factor 1 eV = 8 065.545 eV [11].

(a)			
Energy (eV) $3b_2 \rightarrow 3s$	Wavenbr. (cm-1)	Assignment	
9.337	75,308	**(0,0)**	ω_4=56±3 meV
9.361	75,502	ν_5	450±20 cm^{-1}
9.393	75,760	$\boldsymbol{\nu_4}$	ω_5=20±2 meV
9.413	75,921	ν_5	160±20 cm^{-1}
9.432	76,074	$2\nu_5$	
9.445	76,179	$\mathbf{2\nu_4}$	
9.486	76,510	$2\nu_5$	
5.503	76,647	$\mathbf{3\nu_4}$	
9.521	76,792	ν_5	
9.539	76,937	$2\nu_5$	
9.562	77,123	$\mathbf{4\nu_4}$	
9.583	77,292	ν_5	
9.604	77,461	$2\nu_5$	
(b) $1b_1 \rightarrow 3s$			
9.792	78,978	**(0,0)**	ω_4=58±2 meV
9.806	79,090	ν_5	470±20 cm^{-1}
9.827	79,260	$2\nu_5$	ω_5=18±4 meV
9.848	79,429	$\boldsymbol{\nu_4}$	145±30 cm^{-1}
9.862	79,542	ν_5	
9.883	79,704	$2\nu_5$	
9.909	79,921	$\mathbf{2\nu_4}$	

the presence of a doublet. Von Niessen et al. [4] noticed maxima at 13.0 eV and 13.3 eV. By quantum chemical calculations performed in the present work two closely lying ionized states are calculated at IE_{vert}=13.06 eV and 13.44 eV successively and corresponding to $3b_2^{-1}$ and $1b_1^{-1}$ ionization respectively. These results are in good agreement with the experimental data. The associated adiabatic values IE_{ad}=12.77 eV and 13.22 eV will be used for the convergence limits of the Rydberg series.

Only two Rydberg transitions are detected in series converging to 12.77 eV, i.e. at 9.337 eV ($3b_2 \rightarrow 3$ s) and at 10.327 eV ($3b_2 \rightarrow 3p(\sigma)$). The former transition shows a vibrational progression analyzed and assigned in Table 7a. Two vibrations are involved characterized by wavenumbers of 450±20 cm^{-1} (56±3 meV) and 160±16 cm^{-1} (20±2 meV). Within the frame of our model where the ionic state and the Rydberg state converging to it would have about the same geometry, these wavenumbers should be compared with ω_4^+=372 cm^{-1} and ω_5^+=177 cm^{-1} as predicted by quantum chemical calculations for the $\tilde{D}^2B_2$ state of the ion. No experimental values are available for comparison.

Converging to IE_{ad}=13.20 eV a series has been detected and tentatively assigned to the $1b_1 \rightarrow 3$ s transition. The associated vibrational transitions are listed in Table 7b. Also in this Rydberg state two wavenumbers have been pointed out at 470±20 cm^{-1} (58±2 meV) and 145±30 cm^{-1} (18±4 meV). These values are close to those measured for the $3b_2 \rightarrow 3$ s Rydberg transition. By quantum chemical calculations for the $\tilde{E}^2B_1$ state wavenumbers at ω_4^+=402 cm^{-1} and ω_5^+=164 cm^{-1} are predicted in the present work.

5.2.3. Rydberg transitions between 11.0 eV and 15.0 eV (see Fig. 2)

This part of the vacuum UV PAS (recorded with 10 meV increments) is made of broad and weak bands superimposed on a strong continuum as shown in the upper panel of Fig. 2. To attempt to highlight the presence of structure in this part of the spectrum the subtraction method has been applied. The result is shown in the lower panel of Fig. 2 (black curve). Because of the unfavorable signal/noise ratio a slight smoothing by Fourier transform (FFT) has been applied (red curve Sm).

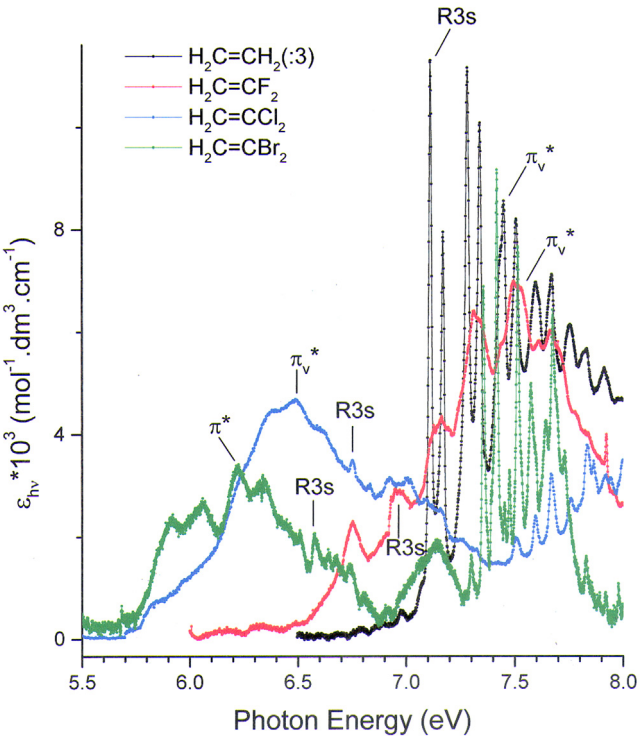

Fig. 8. VUV photoabsorption spectra of C_2H_4 (black), 1,1-$C_2H_2F_2$ (red), 1,1-$C_2H_2Cl_2$ (blue) and 1,1-$C_2H_2Br_2$ (green) on an expanded photon energy scale between 5.5 eV and 8.0 eV. The vertical (index v) and the adiabatic excitation energies of the Rydberg (R3s) transitions are indicated for each molecule.

A broad band extending between 11.4 eV and 12.6 eV is made of several fairly regularly-spaced features. It has been assigned to the $4a_1 \rightarrow 3$ s Rydberg transition with δ=0.975 taking $E_{exc}{}^{ad}$=11.455 eV and the convergence limit at 14.77 eV. The HeI-PES [3] shows a double band extending between 14.4 eV and 17.2 eV. The two maxima are measured at 15.20 eV and 15.85 eV successively [3,4]. These bands are interpreted by the ionization of the $4a_1$ and $2b_2$ MO's successively [4]. Using $E_{exc}{}^{vert}$=11.926 eV and IE_{vert}=15.20 eV [3,4] a quantum defect δ=0.961 is obtained and close to 0.975 obtained from the $E_{exc}{}^{ad}$ value.

Up to 12.321 eV a fairly constant spacing of 160±10 meV (1274±80 cm^{-1}) (bold lines in Fig. 2) is measured. This band also shows a structure with intensity alternation with intervals of 79±6 meV (640±50 cm^{-1}) (dashed lines in Fig. 2). These wavenumbers best compare with $\nu_3{}^+(a_1)$=1115 cm^{-1} and $\nu_6{}^+(a_2)$=613 cm^{-1} predicted for the $\tilde{F}^2A_1$ ionized state by the present calculations.

The calculations carried out in the present work suggest that the situation is actually more complex. Three closely-lying IE_{ad} are calculated at 14.77 eV, 14.97 eV and 15.52 eV. The former is predicted for the $\tilde{F}^2A_1$ state of the ion whereas the two latter are assigned to the $\tilde{G}/\tilde{H}^2B_2$ both being the result of the ionization of the same $2b_2$ MO. The corresponding calculated IE_{vert} are 15.21 eV, 15.85 eV and 15.89 eV respectively.

A next broad band is measured at about $E_{exc}{}^{ad}$=12.73 eV (see Fig. 2). It has likely to be assigned to the $4a_1 \rightarrow 3p$ Rydberg transition with δ=0.42. The last broad band near $E_{exc}{}^{ad}$=14.04 eV (see Fig. 2) could likely be assigned to the Rydberg transition $2b_2 \rightarrow 4$ s/3d, i.e. using IE_{ad}=15.52 eV ($\tilde{H}^2B_2$) a quantum defect δ=0.968/−0.032 is obtained.

6. Conclusions

The use of synchrotron radiation in the vacuum UV enabled us to measure for the first time (i) the PAS of 1,1-$C_2H_2Br_2$ at higher resolution extending the data above the 10.5 eV photon energy limit, i.e., from 10.5 eV to 15 eV and (ii) the PIEC of the parent 1,1-$C_2H_2Br_2{}^+$ and fragment $C_2H_2Br^+$ ions. Applying for the first time quantum chemical calculations to the neutral and ionized states of 1,1-$C_2H_2Br_2$ enabled us to propose assignments to the abundant structure observed in both experiments.

The PIEC of 1,1-$C_2H_2Br_2{}^+$ provided the $IE_{ad}(\tilde{X}^2B_1)$ of the molecular ion at 9.617 eV, IE_{vert}=9.778 eV and the assignment of the observed vibrational structure. The PIEC of the $C_2H_2Br^+$fragment ion shows the probable formation of the Br atom in its two spin-orbit states $^2P_{3/2}$ and $^2P_{1/2}$.

The vacuum UV PAS between 5.6 eV and 11.0 eV has been examined in the light of the results obtained by quantum chemical calculations applied to the neutral and ionized states and the photoionization data. Most of the previous assignments have been revised. Converging to the first ionization limit $\tilde{X}^2B_1$ numerous Rydberg transitions are observed. Many of them show long vibrational progressions. Assignments could be provided on the basis of the vibrational wavenumbers obtained by the quantum chemical calculations presented in this work.

Between 11.0 eV and 15.0 eV the spectrum shows four broad bands. The band extending between 11.5 eV and 12.6 eV likely shows vibrational structure. The three last bands probably converge to the excited $4a_1{}^{-1}$ and $2b_2{}^{-1}$ ionization limits.

At the end of the present study a comparison could be made with our observations at the low-energy side of the vacuum UV PAS of C_2H_4, 1,1-$C_2H_2F_2$ [24] and 1,1-$C_2H_2Cl_2$ [23]. Compared to our observations in bi-halogenated derivatives of ethylene, as shown in Fig. 8, the low-energy band is weaker and extends between 5.7 eV and 7.3 eV. From this comparison the continuous shift to lower energies and the weakening of the $\pi \rightarrow \pi^*$ and $\pi \rightarrow$R3s transitions substituting Br for Cl atoms in the 1,1-position is obvious. Contrariwise a shift to higher energies and a strong intensity increase are induced by substituting F and H atoms for Cl.

Declaration of Competing Interest

The authors declare that they have no known competing financial interests or personal relationships that could have appeared to influence the work reported in this paper.

CRediT authorship contribution statement

R. Locht: Conceptualization, Investigation, Validation, Resources, Data curation, Writing – review & editing, Funding acquisition. **D. Dehareng:** Methodology, Software, Formal analysis, Data curation, Funding acquisition.

Data availability

No data was used for the research described in the article.

Acknowledgments

We are indebted to the University of Liège and to the European Community for financial support. D.D.'s contribution was supported by the Belgian program on Interuniversity Attraction Poles of the Belgian Science Policy (IAP R II 3 CT-2004-506008 P6/19).

Supplementary materials

Supplementary material associated with this article can be found, in the online version, at doi:10.1016/j.jqsrt.2023.108626.

References

[1] Carpenter L.J., Reimann S. (Lead Authors), Scientific assessment of ozone depletion: 2014, Chapter I, "Update on Ozone-depletion substances (ODSs) and other gases of interest to the montreal protocol." pp. 1.50, http://www.wmo.int/pages/prog/arep/gaw/ozone2014/ozone_asst_report.html
[2] Schander J, Russell BR. J. Amer. Chem. Soc. 1976;98:6900.
[3] Wittel K, Bock H. Chem. Ber 1974;107:317.
[4] Von Niessen W, Åsbrink L, Bieri G. J. Electr. Spectry. Rel. Phenom 1982;26:173.
[5] Hoxha A, Locht R, Leyh B, Dehareng D, Hottmann K, Jochims HW, Baumgärtel H. Chem.Phys 2000;260:237.
[6] Locht R, Dehareng D, Hottmann K, Jochims HW, Baumgärtel H, Leyh B. J. Phys. B: At. Mol. Opt. Phys. 2010;43:105101.
[7] Locht R, Dehareng D, Leyh B. AIP Adv 2019;9:015305.
[8] Locht R, Dehareng D, Leyh B. J. Quant. Spect. Rad. Trans 2020;251:107048.
[9] Marmet P. Rev. Sci. Instrum. 1979;50:79 Carbonneau R., Bolduc E., Marmet P., *Can.J.Phys.* **51** (1973) 505; Carbonneau R., Marmet P., *Can.J. Phys.* **51** (1973) 2203; ibid. *Phys.Rev.* A **9** (1974) 1898.
[10] Lofthus A, Krupenie PH. J. Phys. Chem. Ref. Data 1977;6:113.
[11] Tiesinga E, Mohr PJ, Newell DB, Taylor BN. J. Phys. Chem. Ref. Data 2021;50:033105 Mohr P.J., Newell D.B., Taylor B.N., *Rev.Mod.Phys.* **88** (2016) 035009.
[12] Frisch MJ, Trucks GW, Schlegel HB, Scuseria GE, Robb MA, Cheeseman JR, Scalmani G, Barone V, Mennucci B, Petersson GA, Nakatsuji H, Caricato M, Li X, Hratchian HP, Izmaylov AF, Bloino J, Zheng G, Sonnenberg JL, Hada M, Ehara M, Toyota K, Fukuda R, Hasegawa J, Ishida M, Nakajima T, Honda Y, Kitao O, Nakai H, Vreven, Montgomery JA Jr., Peralta JE, Ogliaro F, Bearpark M, Heyd JJ, Brothers E, Kudin KN, Staroverov VN, Kobayashi R, Normand J, Raghavachari K, Rendell A, Burant JC, Iyengar SS, Tomasi J, Cossi M, Rega N, Millam JM, Klene M, Knox JE, Cross JB, Bakken V, Adamo C, Jaramillo J, Gomperts R, Stratmann RE, Yazyev O, Austin AJ, Cammi R, Pomelli C, Ochterski JW, Martin RL, Morokuma K, Zakrzewski VG, Voth GA, Salvador P, Dannenberg JJ, Dapprich S, Daniels AD, Farkas O, Foresman JB, Ortiz JV, Cioslowski J, Fox DJ. *Gaussian 09*, revision A.02. Wallingford CT: Gaussian, Inc; 2009.
[13] Dunning TH Jr.. J. Chem. Phys. 1989;90:1007.
[14] Zhao Y, Truhlar DG. Theor. Chem. Acc. 2008;120:215.
[15] Van Caillie C, Amos RD. Chem. Phys. Lett. 2000;317:159.
[16] de Hemptinne M, Velghe C, Van Riet R. Bull. Cl. Sc. Acad. Roy. Belg. 1944;30:40.
[17] Momigny J. Bull. Soc. Chim. Belg 1961;70:241.
[18] Locht R, Dehareng D, Leyh B. J. Phys. Commun 2017;1:055030 (1,1-); ibid. *J.Electr.Spectry.Rel.Phenom* **247** (2021) 147033 (trans-1,2-); ibid. *unpublished results* (cis-1,2-).
[19] Moore CE. Atomic energy levels, 2, Washington DC: US Gvt Print.Off.; 1952. Circ.Nat.Bur.Stand. **467**.

[20] Gridelet E, Dehareng D, Locht R, Lorquet AJ, Lorquet JC, Leyh B. J. Phys. Chem 2005;109:8225.
[21] Locht R., Leyh B., Jochims H.W., Baumgärtel H., *BESSY Jahres Bericht* 2006 372, http://hdl.handle.net/2268/596: see also "UV/Vis+ Photochemistry Database" (www.Photochemistry.org).
[22] Sarma VN, Yoshi YN. J. Phys. B: At. Mol. Opt. Phys. 1983;16:1671.
[23] Locht R, Dehareng D, Leyh B. J.Phys.Commun 2017;1:045013.
[24] Locht R, Jochims HW, Leyh B. Chem. Phys 2012;405:124.
[25] Robin MB. Higher excited states of polyatomic molecules, I. New York: Academic Press Inc.; 1974.